Pulse shaping and energy storage capabilities of angularly-multiplexed KrF laser fusion drivers

R. H. Lehmberg

Research Support Instruments, Inc., Lanham, MD 20706

J. L. Giuliani and A. J. Schmitt

Plasma Physics Division, U.S. Naval Research Laboratory, Washington, DC 20375

Abstract

This paper describes a rep-rated multi-beam KrF laser driver design for the 500 kJ inertial fusion test facility (FTF) recently proposed by NRL, then models its optical pulse shaping capabilities using the Orestes laser kinetics code. It describes a stable and reliable iteration technique for calculating the required pre-compensated input pulseshape that will achieve the desired output shape, even when the amplifiers are heavily saturated. It also describes how this pre-compensation technique could be experimentally implemented in real time on a rep-rated laser system. The simulations show that this multibeam system can achieve a high fidelity pulse shaping capability, even for a high gain shock ignition pulse whose final spike requires output intensities much higher than the ~ 4 MW/cm^2 saturation levels associated with quasi-cw operation; i.e., they show that KrF can act as a storage medium even for pulsewidths ~ 1 ns. For the chosen pulse, which gives a predicted fusion energy gain ~ 120, the simulations predict the FTF can deliver a total on-target energy of 428 kJ, a peak spike power of 385 TW, and ASE prepulse contrast ratios $I_{ASE}/I < 3 \times 10^{-7}$ in intensity and $F_{ASE}/F < 1.5 \times 10^{-5}$ in fluence. Finally, the paper proposes a front-end pulse shaping technique that combines an optical Kerr gate with cw 248 nm light and a 1 μm control beam shaped by advanced fiber optic technology, such as the one used in the National Ignition Facility (NIF) laser.

PACS numbers: 42.55.Lt; 52.57.-z

Keywords: Inertial fusion energy; Pulse shaping; KrF lasers; Shock ignition

I. INTRODUCTION

One of the primary requirements for laser-driven inertial fusion energy (IFE) is the ability to produce high energy pulses with the temporal shapes needed to control hydrodynamic instabilities and target preheat[1] or to drive shock ignition.[2] Although this capability has been well established on solid state lasers such as the National Ignition Facility (NIF),[3] it is less certain on Krypton Fluoride (KrF) lasers[4]-[10], where the large multi-beam angularly-multiplexed amplifiers tend to have high gains, heavy saturation, and complicated gas kinetics.[11], [12] The high gains may allow excessive preheat due to near-axial amplified spontaneous emission (ASE) and the saturation can produce severe pulse distortion. In this paper, we review the steps required to minimize ASE and pulse distortion, and describe and simulate a robust technique to produce virtually any desired target pulseshape by precompensating the residual distortion. Although this precompensation technique is applicable to any KrF laser, the simulations presented here apply to the large KrF system designed for the recently proposed Fusion Test Facility (FTF).[13] The FTF design has continued to evolve[14] since the original proposal, but the amplifier loading and stage gains remain similar; here, we apply the simulations to the original design, where the staging has been worked out in more detail. The simulation code that allows this design is based on technologies developed by the Nike[4] and Electra[5] laser programs at the Naval Research Laboratory (NRL), in collaboration with other research groups and industry. Nike has achieved routine operation of a high-energy laser target facility[15], extremely uniform target illumination[4],[16] and effective control of ASE.[17] Electra has already achieved continuous rep-rated operation at 2.5 Hz for up to 90,000 shots[14], and has demonstrated a path to sufficiently high efficiency and reliability for laser based inertial fusion energy (IFE).[5]

A conceptual design of the original FTF[13] is shown in Fig. 1. In this design, twenty identical KrF laser systems, each with an output energy up to 28 kJ/pulse distributed in 90 beams, illuminate a spherical shell target at the center of a 5.5 m radius reaction chamber at a rep rate of 5 Hz. This gives a total laser energy of 560 kJ/pulse, which after allowing for a 10% transmission loss, results in a total energy of up to ~ 500 kJ/pulse on target.

Figure 2 shows a schematic view of one of the twenty KrF systems. The front end begins with a rep-rated multi-mode oscillator and beam scrambler, which generates the broadband spatially and temporally incoherent light required for beam profile smoothing by

the induced spatial incoherence (ISI) technique.[18],[4],[8],[9] The light traverses an apodized object aperture, which the laser system images onto the target to produce the required spatial profile. Instantaneously, this profile is random speckle, but the broad laser bandwidth smooths it out to the desired spatial envelope over averaging intervals shorter than the hydrodynamic response times. The aperture is followed by a temporal shaping system that produces a pre-distorted pulse, which the saturated amplifiers mold into the desired shape at the target. This target pulse typically consists of a long ($\sim$ 10 ns) low intensity foot, which ramps up to a shorter ($\sim$ 2.5 ns) high intensity portion.

The individual pulse durations, as well as the KrF* excimer quenching time ($<$ 7 ns), are much shorter than the typical durations ($>$ 50 ns) of the e-beam or discharge systems used to pump the laser amplifiers. To overcome this mismatch and ensure efficient amplification, the beams are angularly multiplexed.[6] In the front end, for example, one first splits a single beam into 15 beams, which are sequentially delayed by $\sim$ 2.5 ns. These beams overlap at the second amplifier (Amp 3 in the figure), but propagate at a slightly different off-axis angles. Thus, even though the pulses are in independent beams, the amplifier effectively sees one continuous train of pulses with a total duration of $\sim$ 50 ns. After an additional 6-fold multiplexing, the front end will deliver $\sim$ 10-20 Joules (at a 5 Hz rep rate) in an array of 90 separate beams, each with one pulse sequentially delayed by $\sim$ 2.5 ns.

Again using the angular multiplexing principle, these beams are amplified in two large aperture rep-rated and double-passed KrF stages. Each stage is laterally pumped by opposed high voltage e-beams whose duration ($\sim$ 260 ns) is long enough to include all 90 of the optical beams. A 6×15 array of convex mirrors expands and overlaps the beams at slightly different off-axis angles in the 30×30 cm^2 driver stage (Amp 2), which amplifies the resulting 90 sequential pulses to a total energy of $\sim$ 1 kJ within the $\sim$ 225 ns flat-top portion of its e-beam pump. The driver's concave rear mirror condenses the beams and directs them through a lens/mirror array, which again expands and overlaps them in the 100×100 cm^2 final stage (Amp 1) located at the driver stage image plane. To satisfy the ISI requirements, both amplifiers, as well as the front end stages, are imaged to the Fourier transform (pupil) plane of the object aperture.[18] The final stage amplifies the sequential pulse train to a maximum total energy of 28 kJ and directs the beams to a recollimation array of smaller ($\sim 20 \times 20$ cm^2) convex mirrors. The pulses in the recollimated beams are then synchronized by a set of optical delay lines (demultiplexing optics) and directed into the focusing optics at

the target chamber. By imposing greater delays on the beams that carry earlier pulses in the amplifiers, the demultiplexing optics enable all the pulses to arrive on target simultaneously.

In order to achieve the full output at high intrinsic efficiency (12%),[13] the final amplifier must operate under highly saturated conditions; in fact even the driver stage will be moderately saturated. The contiguous stacking of the pulses ensures continuous loading of the amplifiers, thereby minimizing ASE and distortion. In principle, one could achieve a constant loading and thereby eliminate distortion entirely by using simple rectangular or symmetric trapezoidal pulses;[11] for the complicated pulseshapes required of KrF drivers, however, it will remain necessary to pre-distort the input pulses. One of the key results that we show here is that if these input pulses all have the *same* pre-distorted shape, then all 90 of the target beam pulses will remain close to the desired shape, in spite of small amplifier gain variations (e.g., due to factors such as fluorine burnup) over the $\sim$ 225 ns flat pump interval. The second key result is that KrF can act as an energy storage medium over times of a few nanoseconds; this allows one to amplify a train of shock ignition pulses, whose intense spikes are separated by a $\sim$ 2.5 ns spacing, without a large energy loss or degradation of pulseshape fidelity.

In the remainder of this paper, we describe our numerical techniques, present the pulse shaping results for the FTF, and propose a versatile technique to form the required pre-distorted front end pulses without the limitations of conventional Pockels cells. Section II describes the simulation code, the general conditions used to model the FTF, and the iteration technique used to calculate the pre-distorted pulse into the driver stage. Section III discusses the results, which show high fidelity generation of a shock ignition pulse and low ASE at the target. Section IV describes the proposed front end pulse forming technique, which combines 1 μm fiber optic technology with an optical Kerr gate to generate the ISI pre-distorted pulseshape at 248 nm. Finally, Sec. V summarizes the results and suggests further work.

II. SIMULATION CODE AND FTF MODEL

A. Orestes code:

We have developed a time-dependent physics simulation code as a tool for the design of KrF laser systems that can serve as IFE drivers. This code, called Orestes, addresses gas kinetics, ASE cell extraction, pulse shaping, and system scaling.[13],[19] The e-beam deposition, including ionization and excitation of the laser gas, is calculated with a Boltzmann code for the electron distribution function.[20] Orestes has spatial resolution for the gas kinetics and laser transport along the lasing axis and computes the gas, electron, and optical energy equations subject to enthalpy balance among the constituents. It follows 24 species with over 140 reactions, including inter- and intra-manifold relaxation of 53 vibrational levels within the KrF excimer. This extends the work of Kannari et al.[12] and accounts for partial depletion of the lower lasing (B) levels due to high laser intensity spikes. The fundamental time step is based on the optical transit time across a single zone along the lasing (z) axis; this allows an exact calculation of the evolving laser pulse shape using the method of characteristics, thereby giving stable and accurate solutions, even with relatively large time steps. For the pulseshape simulations presented here, the spatial grid size is $\Delta z = 2.5$ cm, thus giving a temporal resolution of $\Delta t = \Delta z/c = 83$ ps.

In large amplifiers, it is important to understand the impact of the ASE. This is accomplished in Orestes with a 3-D, time-dependent algorithm that uses a ray trace to describe the off-axis transport along a set of several hundred discrete rays (ordinates);[19] the resulting ASE intensity is approximately uniform in the transverse directions, and can therefore be averaged to give its effective z-dependence. The ASE is also resolved in the frequency domain to account for gain narrowing effects. Orestes has been validated on several KrF lasers over a wide range of parameters. These lasers include the single-pass amplifier at Keio University[21], the 60 cm aperture double-pass main amplifier of Nike,[11] and the 30 cm main Electra amplifier operating as an oscillator[22].

To model high energy angularly multiplexed KrF systems, we have extended Orestes to simulate multistage amplifiers with multiple overlapping beams that can carry independent input pulses. These beams cross at the amplifiers, so if each beam carries one suitably delayed short pulse, the amplifier will see a train of contiguous (or nearly contiguous) pulses that extract energy continuously over most of its e-beam pump duration. As long as the crossing angles are only a few milliradians, one can ignore beam walkoff effects within the amplifiers and continue to use 1D simulations. Thus, the numerical algorithm represents each beam as a separate channel that fills the entire amplifier aperture. At the input of the

first multiplexed stage, it introduces a series of short pulses that are identical to one another, with one sequentially delayed pulse per channel. It then calculates the gain of each channel in that amplifier and uses the resulting output, with suitable attenuation and scaling, as the input to the next stage. As in the usual Orestes algorithm, it evaluates the amplifier saturation from the total instantaneous intensity, which is now obtained by summing over all the channels. The multistage/multibeam capability of Orestes has been benchmarked against measurements of the low level prepulse in Nike target experiments.[17] For simplicity, the simulations are restricted to the last two stages of the FTF laser; i.e., Amp2 and Amp1 shown in the highlighted section of Fig. 2. The model can be readily extended to include the front end, but that complication would add little to the discussion because the front end has low saturation and therefore causes minimal additional distortion.

In the simulations presented here, we chose a train of 90 angularly-multiplexed target beams with a periodicity $t_P = 2.42$ ns, which fills the 223 ns flat-top portion of the e-beam pump, plus a separate axial buffer beam comprised of twelve identical stacked pulses before and six after the target beams. This buffer beam (not shown in Fig. 2) ensures that the amplifiers remain loaded down over almost the entire pump duration, thereby suppressing early-time ASE and providing an "impedance match" to minimize pulse distortion in the first and last few target beams.

Because of its large angular divergence and cw time dependence, ASE can reach the target prematurely and thus preheat it via the demultiplexing optics in the beam channels reserved only for earlier pulses,[17] as illustrated in Fig. 3. This "cross-talk" can also arise from beam to beam scattering at the amplifiers, but it can be kept at a low level by minimizing etching and particulate deposition on the windows. The problem is potentially most serious for ASE generated by the driver stage because that light is further amplified in the final stage. To a good approximation, the total ASE power on target from each of the 20 laser systems is[11]

$$P_{ASE}(t) \simeq 2 \times 10^4 G_D(t)\, G_F(t)\, T N_B(t)\, D_D^2 \Delta\Omega_D(t) \quad \text{Watts}, \tag{1}$$

where $G_D(t)$ and $G_F(t)$ are the respective gains of the driver and final stages, T is the net transmission of the passive optics, $N_B(t)$ is the temporally increasing number of demultiplexed beams whose paths allow light to reach the target at time t, $D_D = 30$ cm is the driver aperture, and $\Delta\Omega_D(t)$ is the solid angle subtended by the target as seen from the driver. The latter can be related to the solid angle $\Delta\Omega_F(t)$ as seen from the final focusing optics by the

well known expression $D_D^2 \Delta\Omega_D(t) = D_F^2 \Delta\Omega_F(t)$, where D_F is the recollimated beam width, $\Delta\Omega_F(t) = \pi R_T^2(t)/f^2$, $R_T(t)$ is the target radius, and f is the focal length. Combining these results, we obtain the total on-target ASE intensity from all 20 laser systems:

$$I_{ASE}(t) = 20\frac{P_{ASE}(t)}{4\pi R_T^2(t)} \simeq 10^5 \frac{G_D(t)\, G_F(t)\, T}{f_\#^2} N_B(t) \ , \tag{2}$$

where $f_\# = f/D_F$ is the f-number of the focusing optics. The time variation of the gain product $G_D(t)\, G_F(t)$ arises from both the e-beam variation and amplifier saturation by the optical beams. The strong variation due to the latter effect is discussed more fully in reference[17] .

B. Iteration technique:

Before starting the iteration technique, one must first estimate how much energy can be extracted from the final amplifier within reasonable constraints on the energy into the driver stage. An input energy > 30 J might require an additional amplifier in the front end, while a choice of < 5 J would require higher driver stage gain and therefore introduce more ASE. Because of amplifier saturation, even small changes in the estimated output energy would require much larger fractional changes in the input, so the best strategy is to shoot for an input energy ~ 10 J. The estimate can be carried out with minimal computation time by first using only a *single* beam with a rectangular 225 ns pulse in place of the 90 target beams. One then chooses the desired pulseshape and scales its intensity $I_S(t)$ to give the above estimated output energy in those beams.

In the 0th iteration, we choose *all* of the $b = 1, \cdots, 90$ driver amplifier input pulses $I_{IN}^{(0)}(b, t - bt_P)$ to be the same shape as the desired output, but delayed by time bt_P and scaled down to the smaller input energy; i.e., $I_{IN}^{(0)}(b, t - bt_P) = \beta I_S(t)$, where $\beta \ll 1$. In the highly saturated amplifiers of interest, the resulting calculated output pulses $I_{OUT}^{(0)}(b, t - bt_P)$ at the final stage will generally be distorted and unequal to the desired intensity $I_S(t)$, especially if there is temporally nonuniform loading due to a foot pulse or a spike at the end of a shock ignition pulse.

In the subsequent iterations we choose one of the 90 beams b_{ref} to represent *all* of the others. Ideally, it should be near the middle of the beam train, but the calculations go faster if it is closer to the front, thereby minimizing the number of beams that must be included.

Here we chose $b_{ref} = 34$ and included beams up to $b_{max} = 45$. The iteration strategy replaces the driver stage input pulse in *each* beam b by its partially compensated version; e.g. the first iteration uses

$$I_{IN}^{(1)}(b, t - bt_P) = I_{IN}^{(0)}(b, t - bt_P) \frac{I_S(t)}{I_{OUT}^{(0)}(b_{ref}, t - b_{ref}t_P)} , \tag{3}$$

then repeats the calculation to give the updated output pulses $I_{OUT}^{(1)}(b, t - bt_P)$ from the final amplifier. One then continues this procedure, replacing

$$I_{IN}^{(n)}(b, t - bt_P) = I_{IN}^{(n-1)}(b, t - bt_P) \frac{I_S(t)}{I_{OUT}^{(n-1)}(b_{ref}, t - b_{ref}t_P)} \tag{4}$$

in each input beam, until the Nth iteration, where the final output reference beam $I_{OUT}^{(N)}(b_{ref}, t - b_{ref}t_P)$ is deemed close enough to $I_S(t)$.

Except for their temporal displacements, all the pre-distorted input pulseshapes $I_{IN}^{(N)}(b, t - bt_P)$ are identical to $I_{IN}^{(N)}(b_{ref}, t - b_{ref}t_P)$. This pulse is then stored in a data file and subsequently used to generate all the 90 target beam simulations shown here. In the flat-top portion of the e-beam excitation, almost all of the other pulses $I_{OUT}^{(N)}(b, t - bt_P)$ should also be close to $I_{OUT}^{(N)}(b_{ref}, t - b_{ref}t_P)$, even with moderate gain variations due to fluorine burn-up or other changes in the gas chemistry. The results presented here confirm this, with only minor distortion in the earliest and latest pulses. No attempt is made to independently pre-correct every beam, although the iteration procedure could be easily modified to do that. Independent pre-correction would allow higher efficiencies by making better use of the rising and falling portions of the e-beam pump pulse, but it would also introduce additional expense and complication in the front end.

Because the amplifiers are highly saturated, large fractional changes in the input intensity result in only small fractional changes at the output. This ensures the stability of the iteration procedure, but it does require a large number of iterations. The number can be reduced significantly by enhancing the correction factor, i.e. replacing expression (4) by

$$I_{IN}^{(n)}(b, t - t_b) = I_{IN}^{(n-1)}(b, t - bt_P) \left[\frac{I_S(t)}{I_{OUT}^{(n-1)}(b_{ref}, t - b_{ref}t_P)} \right]^K , \tag{5}$$

typically with $K = 2$ in the first few iterations. Most of the simulations converge to within $< 2\%$ of the ideal pulseshape within ~ 30 iterations, each of which requires about 30 minutes on a Pentium 4 @ 2.6 GHz with Intel Fortran. We initially considered a non-iterative

approach, which simply reverses the signs of the Orestes gain/loss terms and propagates the beams backward, starting at the final amplifier output and working back toward the driver stage input. As expected, this worked well only under lightly saturated conditions.

Although this paper focuses on the iteration technique as a numerical modelling tool, it could also provide a detailed real-time pulse shaping capability on future large rep-rated laser amplifier systems. One would simply digitize the output pulse from a selected beam, use the above relations to compare it with the desired shape, and program the front end pulse forming electronics to pre-distort the next set of rep-rated pulses. If necessary, the process could be carried out independently on each beam, although that would certainly entail additional cost and complexity.

III. RESULTS

Before showing the results for the multibeam two stage system, we briefly describe the conceptual design of the FTF main amplifier module[13] and simulate its performance with a single long trapezoidal input pulse (Fig. 4) . The laser cell has a 100 cm $\times$ 100 cm aperture, a total length of 280 cm, and it is pumped by four pairs of opposed transverse electron beams. The beam voltage and laser gas pressure are adjusted to give a flat deposition profile across the laser cell, and thus a spatially uniform laser-gain profile. A recirculator convects the gas mixture vertically (out of the page) to cool and quiet it between shots. To increase the gain and extraction efficiency, the laser beam is double-passed. These simulations predict that the module can produce as much as 30 kJ in the 225 ns flat portion of the e-beam with a laser input energy around 1 kJ; this corresponds to an intrinsic efficiency η_{INT} = laser output energy/e-beam deposition energy $\simeq$ 12%. For these simulations, the parameters are: 1.1 atm total gas pressure (40% Kr, 0.40% F2, 59.6% Ar), specific e-beam power deposition $P_{EB} = 526$ kW/cc (giving integrated energy deposition of 237 kJ in the flat portion and 277 kJ total), 99% window transmission and 99% rear mirror reflectivity.

To illustrate KrF laser pulse shaping capabilities, we model the generation of a shock ignition pulse[2] by the FTF system. These pulses offer the possibility of high fusion energy gains in direct-drive targets, but they are a challenge to amplify because they have a complicated structure with a wide dynamic range. In general, they begin with a low energy

prepulse spike (picket) followed by a long ($\sim$ 10 ns) low intensity foot pulse, which ramps up to an intermediate intensity pedestal (compression pulse) and ends with a short spike at much higher intensity. The picket and foot pulse shape the target adiabat profile and enhance the implosion stability, while the final spike drives the ignition shock. Direct-drive 1D simulations by Schmitt,[23] have shown that 248 nm light allows shock ignition gains up to $\sim$ 100, even for total on-target energies as low as 250 kJ; however these pulses require very high spike powers ($\sim$ 800 TW). Recent simulations of larger targets irradiated by longer and higher energy ($\gtrsim$ 400 kJ) pulses show energy gains $>$ 130 with more robust ignition and burn conditions, even with spike powers $\lesssim$ 400 TW.[24] The calculations shown here model the generation of one of these longer pulses whose spike timing and peak power were conservatively chosen well within the range of values that gave gains $\sim$ 130, but not at the maximum gain conditions, which were close to the edge of a cliff. This pulse has an on-target energy of 428 kJ and a peak spike intensity of 383 TW. Allowing for a 10% loss in the output optics, this requires only 23.8 kJ from each of the 20 laser systems, which is comfortably below the 28 kJ main amplifier output of the baseline FTF design. To match this requirement and avoid excessive amplifier gains in the last two stages, we reduced the maximum specific e-beam power depositions from the 526 kW/cc shown above to 445 kW/cc. Finally, because of the 83 ps resolution in the Orestes code, we have chosen the picket pulsewidth longer than in Ref.[24]; however, its on-target energy (2.9 kJ) is the same and its125 ps duration remains much shorter than the relevant hydro time scales during that portion of the pulse.

Figures 5a,b show the pre-distorted input pulses at the driver amplifier required to produce the chosen shock ignition pulse in the reference beam at the final stage output. As seen in Fig. 5c, that reference pulse is nearly identical to the ideal shape. At 0.099 J/pulse, the total input energy is 8.9 J in the 90 target beams, plus an additional 1.8 J in the $12 + 6$ pulse buffer beam. The change in pulseshapes shows significant distortion by amplifier saturation during the high energy spike, whose $\sim$ 23 MW/cm^2 peak output intensity is over five times larger than the cw saturation intensity I_{SAT} shown in Fig. 4. For example, the input reference pulse in Fig. 5b shows small spikes at 125.6, 128 and 130.4 ns that are not seen in the output pulse; as Fig. 5a shows (for beam 1), these spikes are required to compensate the transient saturation due to the final spike of the previous pulse. Similarly, the decreasing input intensity between 131 and 132.5 ns occurs because the saturated amplifier is still recovering from that earlier spike, with a recovery rate that remains somewhat larger

than the saturation rate due to energy currently being extracted.

Figure 6 shows how the output pulses and ASE evolve over the course of the e-beam pump duration. Because of the shortness and high intensity of the spike, the total intensity I_{TOT} (and therefore the loading) is no longer even approximately constant, as it was in Ref [11]; this leads to the periodic ASE fluctuations seen in Fig. 6a. In spite of the variable loading, however, the pulseshape fidelity remains good over all 90 of the target beams. It is clear from Figs. 6b,c that the buffer beam (black line in 6b) not only controls the early-time ASE, but also provides the "impedance match" necessary to ensure good pulseshape fidelity in even the first and last few target beams.

Figure 7 shows the total instantaneous power $P(t)$ and fractional RMS beam-to-beam deviation $\Delta P_{RMS}/P$ in all 90 target beams from each of the 20 laser systems. Part of this deviation is associated with variation in the total energies of the beams, due to slow changes in the KrF kinetics. The total output energy is 23.8 kJ with an average of 264 J/beam and $< 2.5\%$ RMS deviation. Note that this 23.8 kJ is close to the $30.1 \times 445/526 = 25.5$ kJ that one would obtain by scaling the 30.1 kJ flat-top energy shown in Fig. 4 to the lower specific e-beam power depositions (445 kW/cc) used in these simulations, in spite of the fact that the corresponding total input energy to the final stage is significantly lower than in Fig. 4. (720 J vs 1.03 kJ). This clearly demonstrates that the KrF medium is acting as a storage laser over times ~ 1 ns, saving enough energy during the plateau to still drive the spike at the end. Adding all 20 laser systems and allowing for a 10% loss in the output optics, we then obtain a total on-target energy of $20 \times 0.9 \times 23.8$ kJ $= 428$ kJ and respective peak and pedestal powers $20 \times 0.9 \times 21.4$ TW $\simeq 385$ TW and $20 \times 0.9 \times 7.9$ TW $\simeq 142$ TW, in good agreement with the pulses used in Ref.[24].

Figure 8 compares the total on-target pulse and ASE intensities I and I_{ASE}, respectively, along with the corresponding fluences F and F_{ASE}. Again allowing for a 10% loss in the output optics, we obtain I_{ASE} from Eq. (2) with output transmission $T = 0.9$, and the pulse intensity $I(t)$ from the expression

$$I(t) = 20\frac{0.9P(t)}{4\pi R_T^2(t)}\ , \tag{6}$$

where the beam radius $R_T(t)$ zooms down to 63% its initial 1.08 mm size at the beginning of the pedestal and 41% at the beginning of the spike, as specified in the target simulations.[24] This zoom, which is responsible for the enhanced intensity jumps at the pedestal and spike,

can be readily accomplished with ISI by shunting different portions of the oscillator pulse through different sized object apertures in the front end.[18] (Note that the zoom has no effect on the overall beam sizes in the pulse-shaping optics and amplifiers, which lie at Fourier transform planes of the object apertures.) The comparisons show that $I_{ASE}/I < 3 \times 10^{-7}$ and $F_{ASE}/F < 1.5 \times 10^{-5}$ at all times during the pulse, except for the dead zone just after the initial spike, where the ASE fluence is less than 0.25 J/cm^2. If lower ASE is required, it can be accomplished by doubling the input energy to the driver stage, thereby reducing the total gain product in Eq. (2) and slightly increasing the output energy.

As seen in Fig. 2, the last amplifier in the front end (Amp 3) is also angularly-multiplexed, and would therefore be capable of introducing additional on-target ASE unless steps are taken to suppress it. This stage would introduce an additional gain ~ 10 in Eq. (2), but it handles only 15 beams instead of 90; hence its contribution would be approximately $10 \times 15/90 \simeq 1.7$ times that of the driver stage (Amp 2). Fortunately, the apertures of these beams are still small enough to allow a Pockels cell in each one to suppress the ASE shortly before and after the pulse that it carries.

IV. FRONT END PULSE SHAPING SYSTEM

To generate the complicated pre-distorted input pulses required at the front end, we propose a versatile fiber electro-optic technique that avoids most of the limitations of conventional Pockels cells. Fiber optic pulse shaping techniques are best suited for coherent light at wavelengths in the near-IR. We propose to take advantage of the advanced fiber electro-optic technology developed for the National Ignition Facility[3] (NIF) to shape a coherent 1 μm pulse, then use that pulse as a control beam to impose the desired temporal shape on a cw 248 nm ISI beam via an optical Kerr gate. As illustrated in Fig. 9, an initially x-polarized cw 248 nm ISI beam E_I mixes with a co-propagating pulsed coherent 1 μm phase control beam E_C polarized at 45° in the x-y plane. (The analysis can also apply to the case where the two beams have a small crossing angle $<<$ 1 rad in the x-z plane.) The four-wave mixing process allows E_C to induce a time-dependent birefringence that rotates the polarization of E_I through an angle $\theta(t)$. This imposes the desired temporal pulse envelope on the ISI beam E_{Iy} at the output of the y polarizer, whose transmission is $T_y(t) = \sin^2\theta(t)$,where $\theta(t) = \phi(t)/2$ is determined by the nonlinear differential phase

shift $\phi(t)$. If the ISI intensity remains small compared to the 1 μm intensity $I_C(t)$, then[25]

$$\phi(t) \simeq 24\pi^2 \times 10^{16} \frac{L\omega_I}{c^2 n_C n_I} \left[\chi_{xxyy}(\omega_I) + \chi_{xyyx}(\omega_I)\right]_{\rm cgs} I_C(t) \ , \tag{7}$$

where L is the length of the cell in cm, $I_C(t)$ is expressed in GW/cm^2, (n_C , n_I) are the respective refractive indices of the control and ISI beams, (ω_C, ω_I) are the respective frequencies, and $\chi_{xxyy}(\omega_I)$, $\chi_{xyyx}(\omega_I)$ are the third order nonlinear optical susceptibilities at the mixing frequency $\omega_I + \omega_C - \omega_C = \omega_I$. Clearly, the best transfer from the control beam to the ISI light occurs when the pulse peaks around $\phi \lesssim \pi$.

To ensure that usable values of $\phi(t) \sim \pi$ can be achieved without appreciable self-focusing of the control beam, one must compare $\phi(t)$ to the control beam's self-induced nonlinear phase shift:[26]

$$B_C(t) = \frac{\omega_C L}{c}\delta n_C = \frac{24\pi^2 L\omega_C}{c^2 n_C^2} \left[\chi_{xxyy}(\omega_C) + \tfrac{1}{2}\chi_{xyyx}(\omega_C)\right]_{\rm cgs} I_C(t) \ , \tag{8}$$

where $\chi_{xxyy}(\omega_C)$, $\chi_{xyyx}(\omega_C)$ is evaluated at the mixing frequency $\omega_C + \omega_C - \omega_C = \omega_C$. The ratio is

$$\eta \equiv \frac{\phi_I(t)}{B_C(t)} = \frac{\chi_{xxyy}(\omega_I) + \chi_{xyyx}(\omega_I)}{\chi_{xxyy}(\omega_C) + \frac{1}{2}\chi_{xyyx}(\omega_C)} \left(\frac{n_C\omega_I}{n_I\omega_C}\right) \ . \tag{9}$$

For the proposed configuration, $n_C\omega_I/(n_I\omega_C) \simeq 4$; this gives $\eta \simeq 5.3$ for nonresonant electronic nonlinearity, where $\chi_{xyyx}/\chi_{xxyy} = 1$, and $\eta \simeq 7.0$ for molecular orientation nonlinearity in a Kerr liquid, where $\chi_{xyyx}/\chi_{xxyy} = 6$. (The response time of Kerr liquids is typically > 1 ps, but that is not a problem here because the nonlinear rotation is driven by only the control beam intensity, which varies much more slowly than the ISI speckle.) In both cases, we can achieve the $T_y(t) = 1$ condition $\phi(t) = \pi$ with only $B_C \sim 0.5$ radian, which would be too small to cause appreciable self focusing. These favorable η values clearly result from the fact that $\omega_I > 4\omega_C$.

Finally, we can use the above result to show that $\phi(t) \simeq \pi$ can be achieved with modest intensities $I_C \sim 1$ GW/cm^2 and total energies $W_C \sim 1$ Joule. One can estimate B_C directly from tabulated nonlinear refractive indices n_2 defined by

$$\delta n_C = 2n_2 |E_C|^2 = 4\pi \times 10^{16} \frac{n_2\,[\text{esu}]\, I_C\left[\text{GW/cm}^2\right]}{cn_C}. \tag{10}$$

For a square beam of width D_C and pulsewidth Δt_C, the peak nonlinear phase shift is

$$B_C = 2.5 \times 10^{11} \frac{n_2\,[\text{esu}]\, W_C\,[\text{J}]\, L}{n_C D_C^2 \Delta t_C\,[\text{ns}]} \ . \tag{11}$$

Assuming a uv-transmitting liquid of modest nonlinear index (e.g., Ethanol, where $n_2 = 2.5 \times 10^{-13}$ esu and $n_C = 1.36$), pulse energy $W_C = 1$ J, propagation path $L = 9$ cm, beam width $D_C = 0.6$ cm (2.8 J/cm^2 fluence) within a pulsewidth $\Delta t_C = 2.5$ ns ($I_C = 1.1$ GW/cm^2), we obtain $B_C \simeq 0.46$. (Note that the RMS electric field required for 1.1 GW/cm^2 is $\sqrt{2 \times 10^9 / (\epsilon_0 c)} \approx 900$ kV/cm, which is too large for flexible subnanosecond pulse shaping using conventional pulsed power techniques.) For molecular rotation in liquids, where $\eta \simeq 7$, we obtain the required phase shift $\phi \approx \pi$. Other uv-transmitting liquids with larger n_2 values will allow similar performance with lower pulse energies and/or shorter propagation paths. E.g., Hexadecane has $n_2 = 15.5 \times 10^{-13}$ esu and $n_C = 1.43$; hence a pulse energy 0.5 J, propagation path 3 cm, beam width 0.6 cm (1.4 J/cm^2), and pulsewidth 2.5 ns gives $B_C \simeq 0.45$ and again $\phi \approx \pi$. The second example would allow a shaped ISI pulse energy as high as 25 mJ with an intensity less than 1/20th of $I_C = 0.56$ GW/cm^2. As an alternative medium, it is also feasible to use a wide bandgap isotropic crystal such as Y_2O_3, where $n_2 = 5.33 \times 10^{-13}$ esu and $n_C = 1.92$.

V. SUMMARY AND FUTURE WORK

This paper has described a rep-rated KrF laser driver design for the 500 kJ inertial fusion test facility (FTF) recently proposed by NRL, and modeled its optical pulse shaping capabilities using the Orestes laser kinetics code. To achieve the desired output pulseshape from the heavily saturated amplifiers, we developed a stable and reliable iteration technique for calculating the required pre-compensated input pulseshape. The results have shown that this multibeam system can achieve a high fidelity shaping capability, even for a high gain shock ignition pulse whose final spike requires output intensities much higher than the $I_{SAT} \sim 4$ MW/cm^2 saturation levels normally associated with quasi-cw operation; i.e., they show that KrF can act as a storage medium even for pulsewidths ~ 1 ns. The iteration technique could also provide a real-time pulse shaping capability on future large rep-rated laser systems. To do this, one would digitize the output pulse from a selected beam, use Eqs. (4) and (5) to compare it with the desired shape, and program the front end pulse forming electronics to pre-distort the next rep-rated input pulse. The simulations show that the FTF design allows energies up to 30 kJ from each of its 20 amplifier systems with low ASE levels. For the shock ignition pulse chosen here, which gives a predicted fusion

energy gain ~ 120, the FTF simulations show a total on-target energy of 428 kJ, a peak spike power of 385 TW, and ASE prepulse contrast ratios $I_{ASE}/I < 3 \times 10^{-7}$ in intensity and $F_{ASE}/F < 1.5 \times 10^{-5}$ in fluence. Finally we have proposed a versatile front end pulse shaping technique that combines an optical Kerr gate with cw 248 nm light and a 1 μm control beam shaped by advanced fiber optic technology, such as the one used in the NIF.

In future work, we will examine three remaining questions.

(i) What are the KrF laser limitations on raising the peak power in the shock ignition spike? Target simulations show that higher spike powers increase the range of allowable shock mistiming under high gain conditions[23], but they put additional stress on the KrF amplifiers and output optics.

(ii) What are the benefits of applying the iteration technique to more than one of the 90 target beams? Applying the iteration technique to several target beams would certainly entail additional cost and complexity, but it could result in significantly higher efficiency. For example, if one could replace half of the twelve leading and six trailing pulses in the buffer beam shown in Fig. 6b by multiplexed target beams, each with its own independently pre-distorted (and more energetic) input pulse, then the flat-top part of the e-beam pump could be shortened and the efficiency increased by $\sim 10\%$.

(iii) Are there any benefits to amplifying the main pulse and shock ignition spike in separate beams? For example, the first 45 target beams could carry the foot and main pulse, while the last 45 would be dedicated to the spike. This would take advantage of the shorter demultiplexing paths of those last 45 beams to reduce nonlinear propagation effects in the spikes, but it would be efficient only for comparable spike and main pulse energies.

Acknowledgments

The authors wish to thank Malcolm McGeoch for his design of the FTF layout, Tom Lehecka for his work on the laser system architecture, and Max Karasik for providing Fig. 3. We also acknowledge valuable discussions with Steve Obenschain and John Sethian. This work was supported by U.S. Department of Energy

[1] S.E. Bodner, D.G. Colombant, J.H. Gardner, R. H. Lehmberg, S.P. Obenschain, L. Phillips, A.J. Schmitt, J.D. Sethian, R.L. McCrory, W. Seka, C.P. Verdon, J.P. Knauer, B. B. Afeyan, and H.T. Powell, "Direct-drive laser fusion: Status and prospects", Phys. Plasmas **5**, 1901-1918 (1998)

[2] R. Betti, C.D. Zhou, K.S. Anderson, L.J. Perkins, W. Theobald, and A.A. Solodov, "Shock ignition of thermonuclear fuel with high areal density," Phys. Rev. Lett. **98**, 155001 (2007); R. Betti, W. Theobald, C.D. Zhou, K.S. Anderson, P.W. McKenty, S. Skupsky, D. Shvarts, V.N. Goncharov, J.A Delettrez, R.B. Radha, T.C. Sangster, C. Stoeckl, and D.D. Meyerhofer, "Shock ignition of thermonuclear fuel with high areal densities," J. of Phys.: Conference Series **112**, 022024 (2008)

[3] C.A. Haynam, et. al., "National Ignition Facility laser performance status" Appl. Optics **46**, 3276-3303 (2007)

[4] S.P. Obenschain, S.E. Bodner, D. Colombant, K. Gerber, R.H. Lehmberg, E.A. McLean, A.N. Mostovych, M.S. Pronko, C.J. Pawley, A.J. Schmitt, J.D. Sethian, V. Serlin, J.A. Stamper, C.A. Sullivan, J.P. Dahlburg, J.H. Gardner, Y. Chan, A.V. Deniz, J. Hardgrove, T. Lehecka, and M. Klapisch, "The Nike laser facility: Performance and initial target experiments," Phys. Plasmas **3**, 2098-2107 (1996)

[5] M.F. Wolford, M.C. Myers, J.L. Giuliani, J.D. Sethian, P.M. Burns, F. Hegeler, and R. Jaynes, "Repetition-rate angularly multiplexed krypton fluoride laser system," Optical Engineering 47, 104202-1-11 (2008); M.F. Wolford, M.C. Myers, J.L. Giuliani, J.D. Sethian, P.M. Burns, F. Hegeler, and R. Jaynes, "Electra: durable repetitively pulsed 700 J, 100 ns electron beam pumped KrF laser system," Proc. SPIE **6454**, 645407 (2007); J.D. Sethian, M.C. Myers, J.L. Giuliani, R.H. Lehmberg, P.C. Kepple, S.P. Obenschain, F. Hegeler, M. Friedman, M.F. Wolford, R.V. Smilgys, S.B. Swanekamp, D. Weidenheimer, D. Giorgi, D. Welch, D.V. Rose, and S. Searles, "Electron Beam Pumped Krypton Fluoride Lasers for Fusion Energy", Proc. IEEE **92**, 1043-1056 (2004)

[6] L.A Rosocha, J.A. Hanlon and J. McLeod, M. Kang, B.L. Kortegaard, M.D. Burrows, and P.S. Bowling, "Aurora multijoule KrF laser system prototype for inertial cinfinement fusion," Fusion Technol. **11**, 497-531 (1987); J.A. Hanlon and J. McLeod, "The Aurora laser optical system,"

Fusion Technol. **11**, 634-653 (1987).

[7] Y. Owadano, I. Okuda, Y. Matsumoto, I. Matsushima, E. Takahashi, E. Miura, H. Yashiro, T. Tomie, K. Kuwahra, and M. Shinbo, "Overview of Super-ASHURA KrF laser program," Fusion Engineering and Design **44**, 91-96 (1999); I. Okuda, E. Takahashi, I. Matsushima, Y. Matsumoto, H. Yashiro, E. Miura, T. Tomie, Y. Owadano, "Performance of the Super-ASHURA main amplifier," Fusion Engineering and Design **44**, 377-381 (1999)

[8] J.M.D. Lister, M.J. Shaw, C.J. Hooker, and E.C. Harvey, "Uniform target illumination by induced spatial incoherence in a multiplexed KrF laser system," Optics Comm. **84**, 55-60 (1991)

[9] Xiang Yi-huai, Gao Zhi-xing, Tong Xiao-hui, Dai Hui, Tang Xiu-zhang and ShanYu-sheng, "Beam-smoothing investigation on 'Heaven I'," Proc. SPIE **6279**, 62795Z (2007)

[10] V.D. Zvorykin, S.V. Arlantsev, R.V. Gaynutdinov, I.V. Kholin, A.O. Levchenko, N.N. Mogilenetz, A.G. Molchanov, V.F. Oreshkin, M.A. Rogulev, S.I. Sagitov, A.P. Sergeev, P.B. Sergeev, D.B. Stavrovskii, N.N. Ustinovskii, and D.A. Zayarnyi, "Quests for Inertial Fusion Energy conducted at GARPUN KrF laser facility," Journal of Physics: Conference Series **112**, 032055 (2008)

[11] M.W. McGeoch, P.A. Corcoran, R.G. Altes, I.D. Smith, S.E. Bodner, R.H. Lehmberg, S.P. Obenschain, and J.D. Sethian, "Conceptual design of a 2-MJ Krf laser fusion facility" Fusion Technology **32**, 610-643 (1997)

[12] F. Kannari, M. Obara, and T. Fujioka, "An advanced kinetic model of electron-beam-excited KrF lasers including the vibrational relaxation in KrF*(B) and collisional mixing of KrF*(B,C)," J. Appl. Phys. **57**, 4309-4322 (1985).

[13] S.P. Obenschain, D.G. Colombant, A.J. Schmitt, J.D. Sethian, and M.W. McGeoch, "Pathway to a lower cost high repetition rate ignition facility," Phys. Plasmas **13**, 056320 (2005); "Stage 1 Program: Development of science & technology for the Fusion Test Facility" Naval Research Laboratory proposal to the USDOE (April 2006) Chapts. 2 and 3

[14] S.P. Obenschain, J.D. Sethian, and A.J. Schmitt, "A laser based fusion test facility," Fusion Science and Technology, in press

[15] C.J. Pawley, K. Gerber, R. H. Lehmberg, E.A. McLean, A.N. Mostovych, S.P. Obenschain, J.D. Sethian, V. Serlin, J.A. Stamper, C.A. Sullivan, S.E. Bodner, D. Colombant, J.P. Dahlburg, A.J. Schmitt, J.H. Gardner, C. Brown, J.F. Seely, T. Lehecka, Y. Aglitskiy, A.V. Deniz, Y. Chan, N. Metzler, and M. Klapisch, "Measurements of laser-imprinted perturbations and Rayleigh-Taylor

growth with the Nike laser," Phys. Plasmas **4**, 1969-1977 (1997)

[16] A.V. Deniz, T. Lehecka, R.H. Lehmberg and S.P. Obenschain, "Comparison between measured and calculated nonuniformities of Nike laser beams smoothed by induced spatial incoherence," Optics Comm. **147**, 402-410 (1998)

[17] Max Karasik, A.N. Mostovych, R.H. Lehmberg, Y. Chan, J.L. Weaver, and S.P. Obenschain, "Measurements of low-level prepulse on Nike KrF laser," J. Appl. Phys. **98**, 053101-053101-8 (2005)

[18] R.H. Lehmberg and J. Goldhar, "Use of incoherence to produce to produce smooth and controllable irradiation profiles with KrF fusion lasers," Fusion Technol. **11**, 532-541 (1987); R.H. Lehmberg, A.J. Schmitt, and S.E. Bodner, "Theory of induced spatial incoherence," J. Appl. Phys. **62**, 2680-2701 (1987)

[19] R.H. Lehmberg and J.L. Giuliani, "Simulation of amplified spontaneous emission in high gain KrF laser amplifiers," J. Appl. Phys. **94**, 31-43 (2003)

[20] G. Petrov, J.L. Giuliani, and A. Dasgupta, "Electron energy deposition in an electron beam pumped KrF amplifier: Impact of beam power and energy," J. Appl. Phys. **91**, 2662-2677 (2002); J.L. Giuliani, G. Petrov, and A. Dasgupta, "Electron energy deposition in an electron beam pumped KrF amplifier: Impact of the gas composition," J. of Appl. Phys. **92**, 1200-1206 (2002)

[21] A. Suda, H. Kumagai, and M. Obara, "Characteristics of an electron beam pumped KrF laser amplifier with an atmospheric-pressure Kr-rich mixture in a strongly saturated region," Appl. Phys. Lett. **51**, 218-220 (1987)

[22] M.F. Wolford, F. Hegeler, M.C. Myers, J.L. Giuliani, and J.D. Sethian, "Repetitively pulsed 500 J, 100 ns, KrF oscillator," Appl. Phys. Lett. **84**, 326-328 (2004)

[23] A.J. Schmitt, "Direct drive fusion energy schock ignition designs for sub-MJ lasers," Fusion Science and Technology, in press

[24] A.J. Schmitt, private communication

[25] R.L. Sutherland, Handbook of Nonlinear Optics, Marcel Dekker, Inc. New York (1966)

[26] R.W. Boyd, Nonlinear Optics, 2nd Edition, Academic Press, Amsterdam (2003)

Figure Captions

Fig. 1 Overview of the proposed Fusion Test Facility (FTF)

Fig. 2 Optical block diagram of the FTF laser architecture for one of the twenty identical systems, each having a total energy up to 28 kJ in 90 single pulse beams with pulses separated by ~2.5 ns

Fig. 3 Double-pass laser amplifier, showing how the broad angular divergence of the ASE allows it to infiltrate all of the beam channels.

Fig. 4 Description and long-pulse performance of the proposed final amplifier module design. Upper Left: Top view of the laser cell, including the e-beam pump configuration. Four sets of opposing e-beams are injected by two cathode pairs on each side with an axial separation of 40 cm. Upper Right: The cathodes in each pair are 50 cm wide × 100 cm high and separated by 10 cm to allow support for the hibachi frames. Lower left: Predicted temporal history of the e-beam P_{EB} and intensities of the input I_{IN}, output I_{OUT}, and ASE I_{ASE}. Lower right: Axial profile snapshots (at 150 nsec) of the e-beams, ASE, internal intensities $I(z)$, and effective saturation intensity I_{SAT}.

Fig. 5 Driver input pulses required to produce the shock ignition pulses at the final amplifier output: (a) First target beam I_1 (blue), front end of the buffer beam I_{BUF} (black) and total input intensity of all beams I_{TOT} (light grey); (b) Input pulse with a magnified time scale; (c) Comparison of the final amplifier output pulse in the reference beam to the (shifted) ideal shock ignition pulse.

Fig. 6 (a,b) Simulated parameters at the final amplifier, showing selected output beams I_1, I_{REF}, I_{90} (blue), buffer beam I_{BUF} (black), total output intensity of all beams I_{TOT} (light grey), total ASE output I_{ASE} (green), and e-beam specific power deposition P_{EB} (red); (c) I_1, I_{REF}, I_{90} and I_{TOT} with magnified time scales.

Fig. 7 Total instantaneous power in all 90 beams (blue) and fractional beam-to-beam RMS deviation (red) of the shock ignition pulse.

Fig. 8 Total on-target intensities (solid lines) and fluences (dashed lines) of the shock ignition pulse (blue) and ASE (green) from all 20 laser systems. The origin of the time scale is placed at the beginning of the picket pulse.

Fig. 9 Configuration of the proposed Kerr gate that uses an intense coherent 1 μm pulse to impose the desired pre-distorted envelope shape on a cw 248 nm ISI beam via polarization rotation.

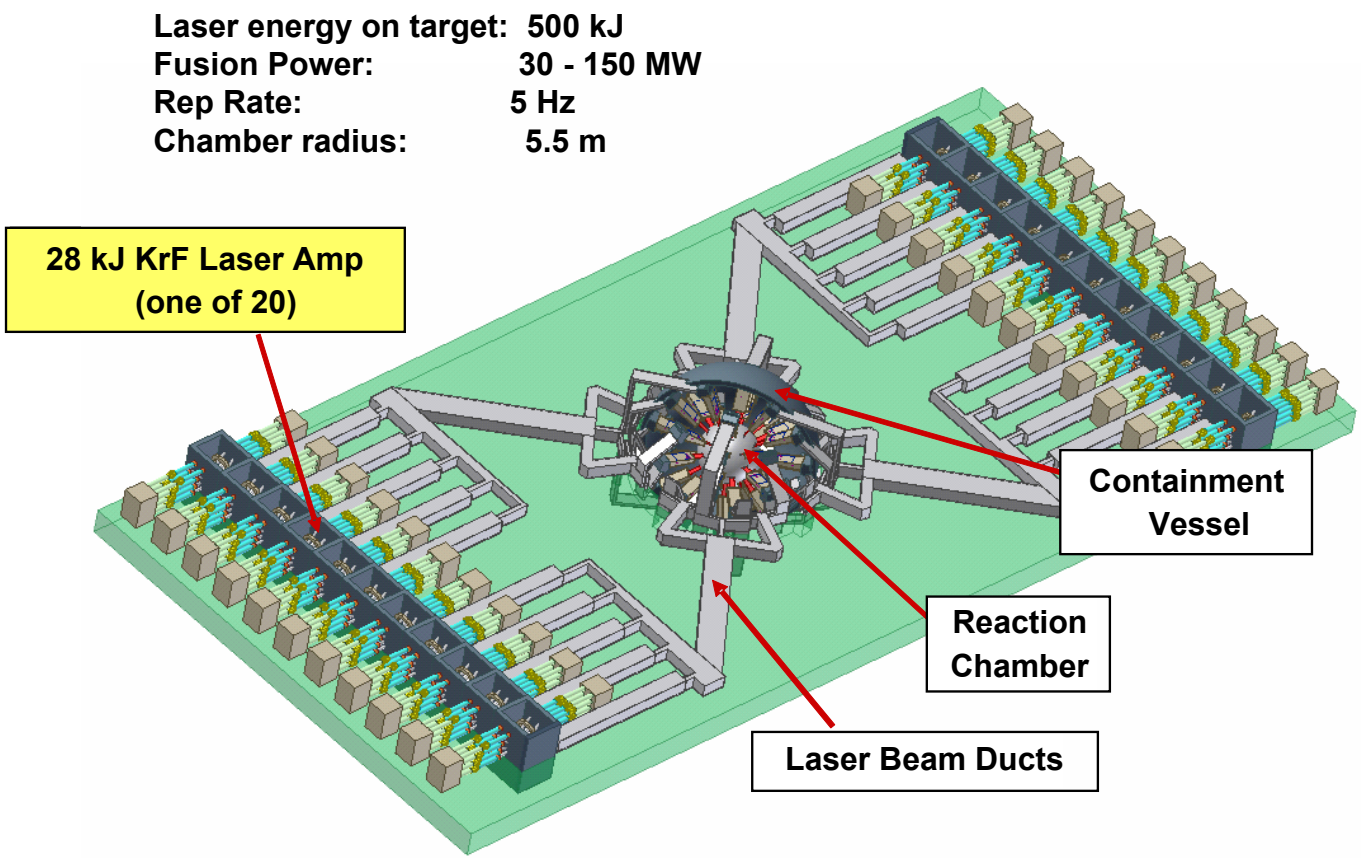

Fig. 1: Overview of the proposed Fusion Test Facility (FTF)

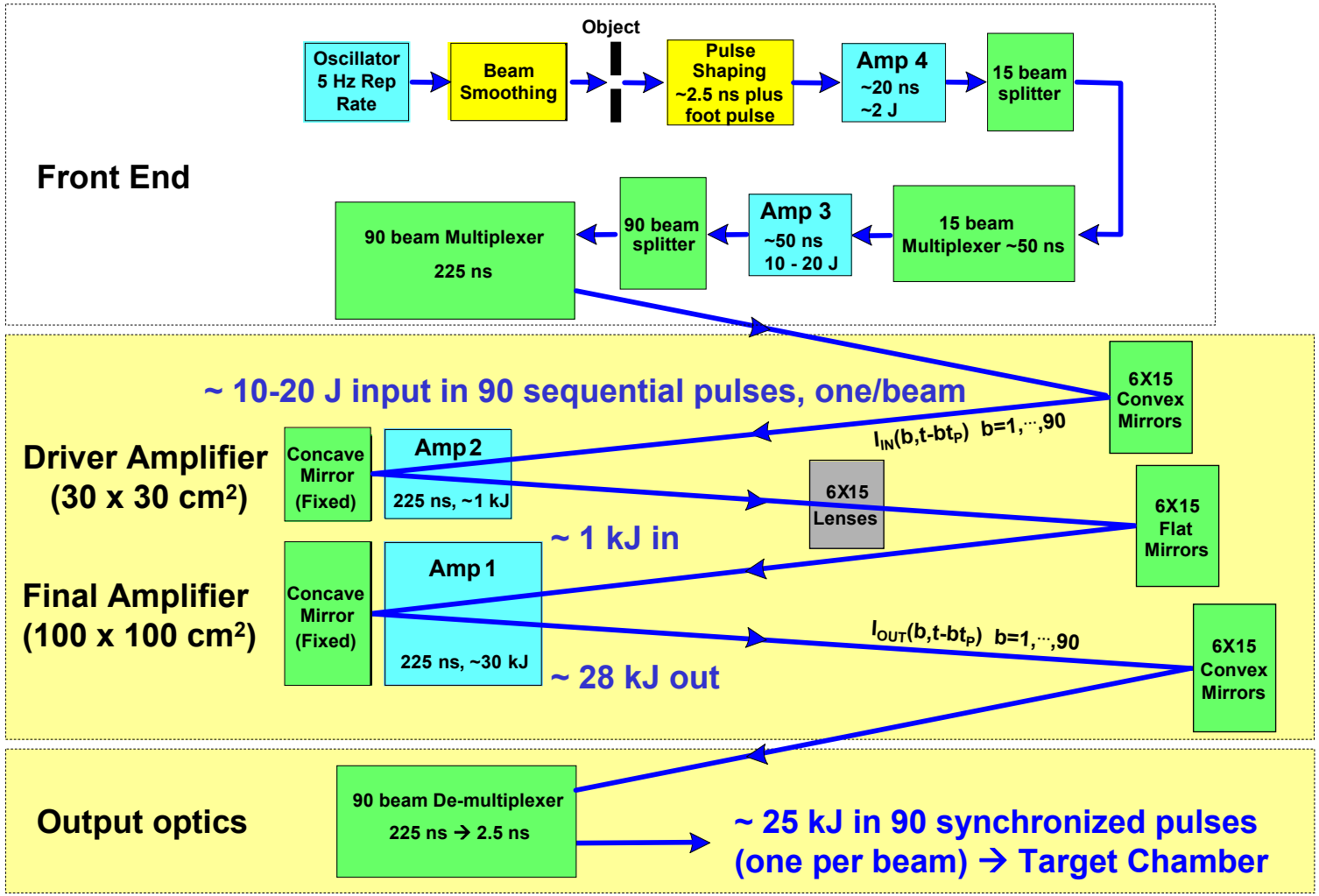

Fig. 2: Optical block diagram of the FTF laser architecture for one of the twenty identical systems, each having a total energy up to 28 kJ in 90 single pulse beams with pulses separated by ~2.5 ns

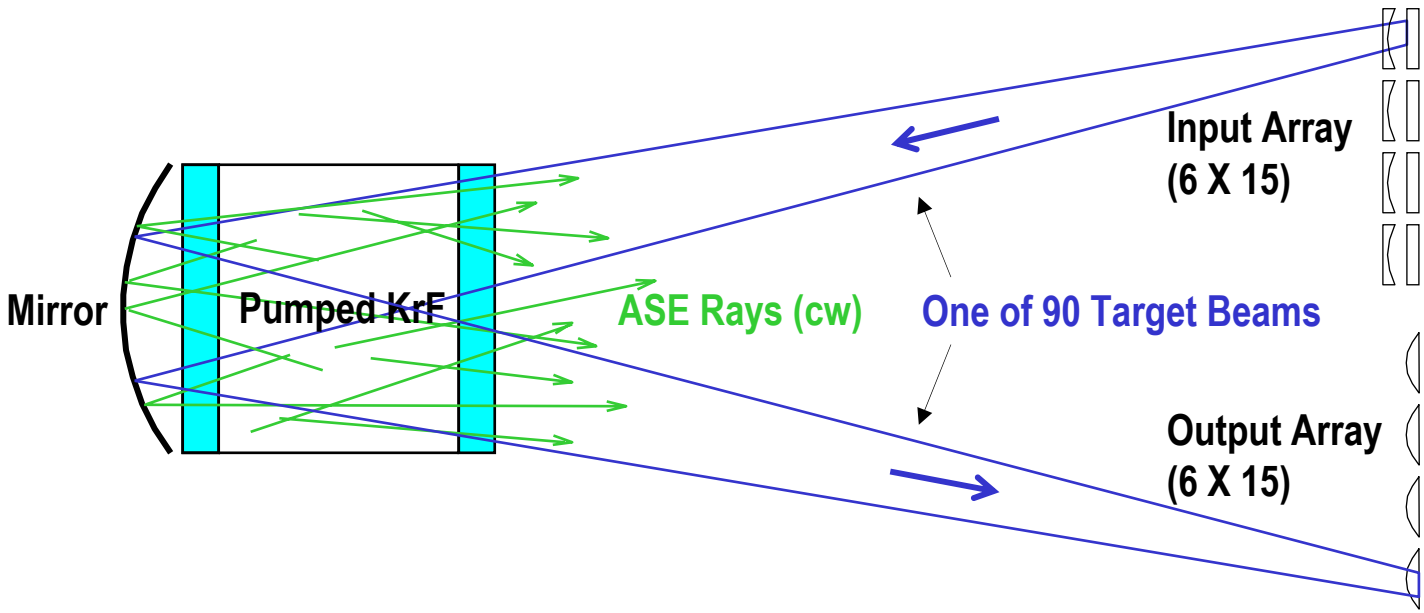

Fig. 3: Double-pass laser amplifier, showing how the broad angular divergence of the ASE allows it to infiltrate all of the beam channels.

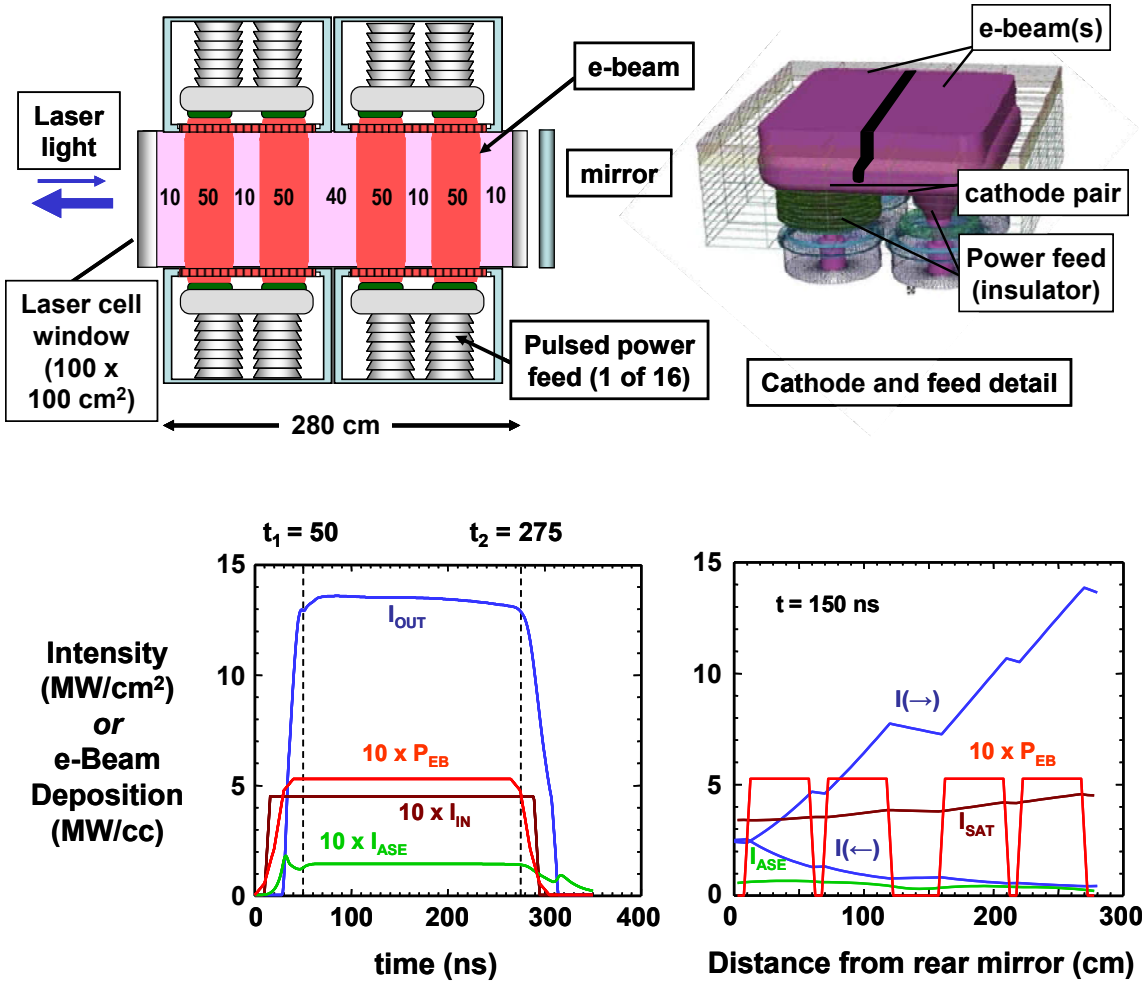

Fig. 4: Description and long-pulse performance of the proposed final amplifier module design. Upper Left: Top view of the laser cell, including the e-beam pump configuration. Four sets of opposing e-beams are injected by two cathode pairs on each side with an axial separation of 40 cm. Upper Right: The cathodes in each pair are 50 cm wide × 100 cm high and separated by 10 cm to allow support for the hibachi frames. Lower left: Predicted temporal history of the e-beam P_{EB} and intensities of the input I_{IN}, output $I_{_OUT}$, and ASE I_{ASE}. Lower right: Axial profile snapshots (at 150 nsec) of the e-beams, ASE, internal intensities I(z), and effective saturation intensity I_{SAT}.

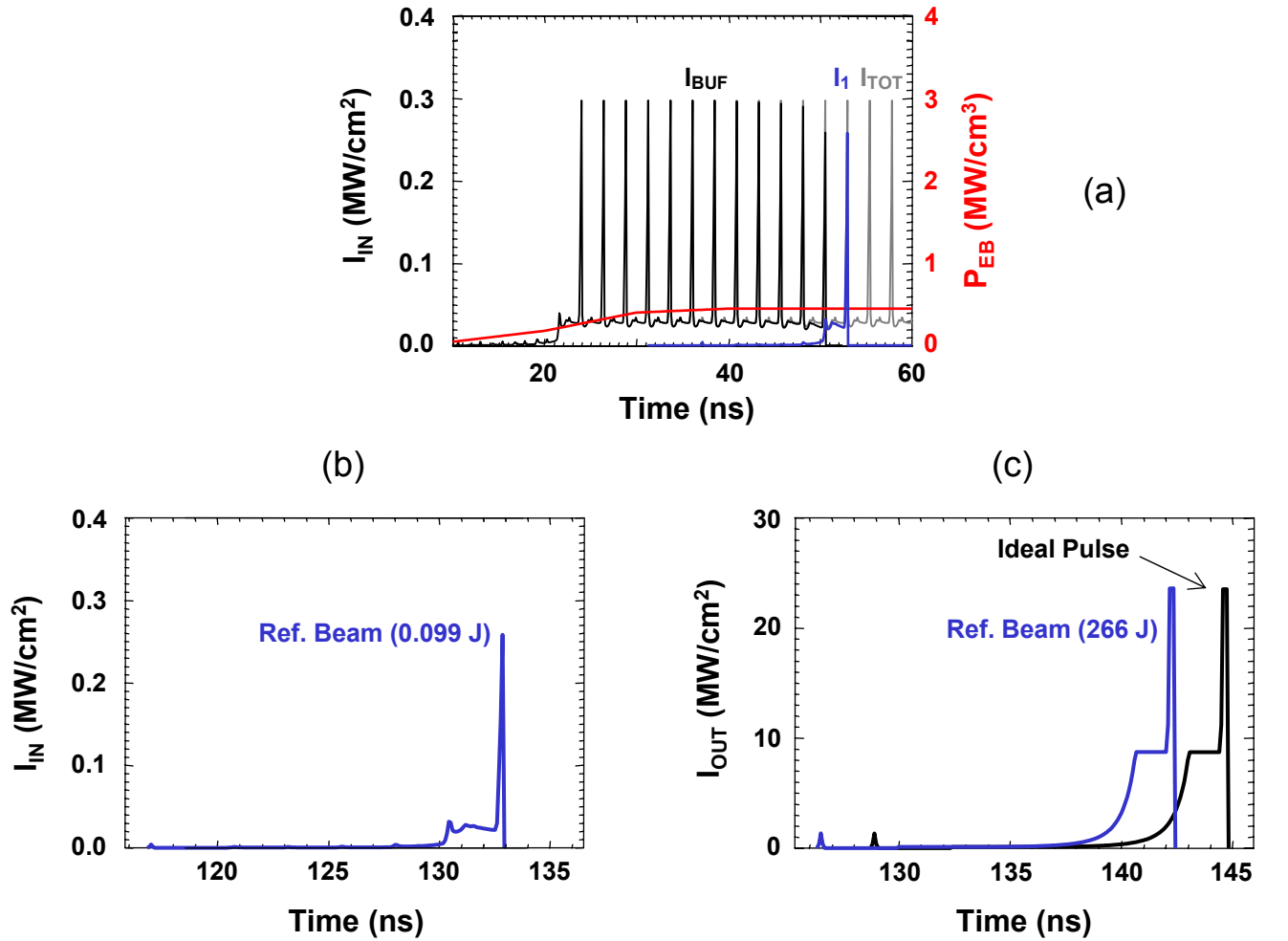

Fig. 5: Driver input pulses required to produce the shock ignition pulses at the final amplifier output: (a) First target beam I_1 (blue), front end of the buffer beam I_{BUF} (black) and total input intensity of all beams I_{TOT} (light grey); (b) Input pulse with a magnified time scale; (c) Comparison of the final output pulse in the reference beam to the (shifted) ideal shock ignition pulse.

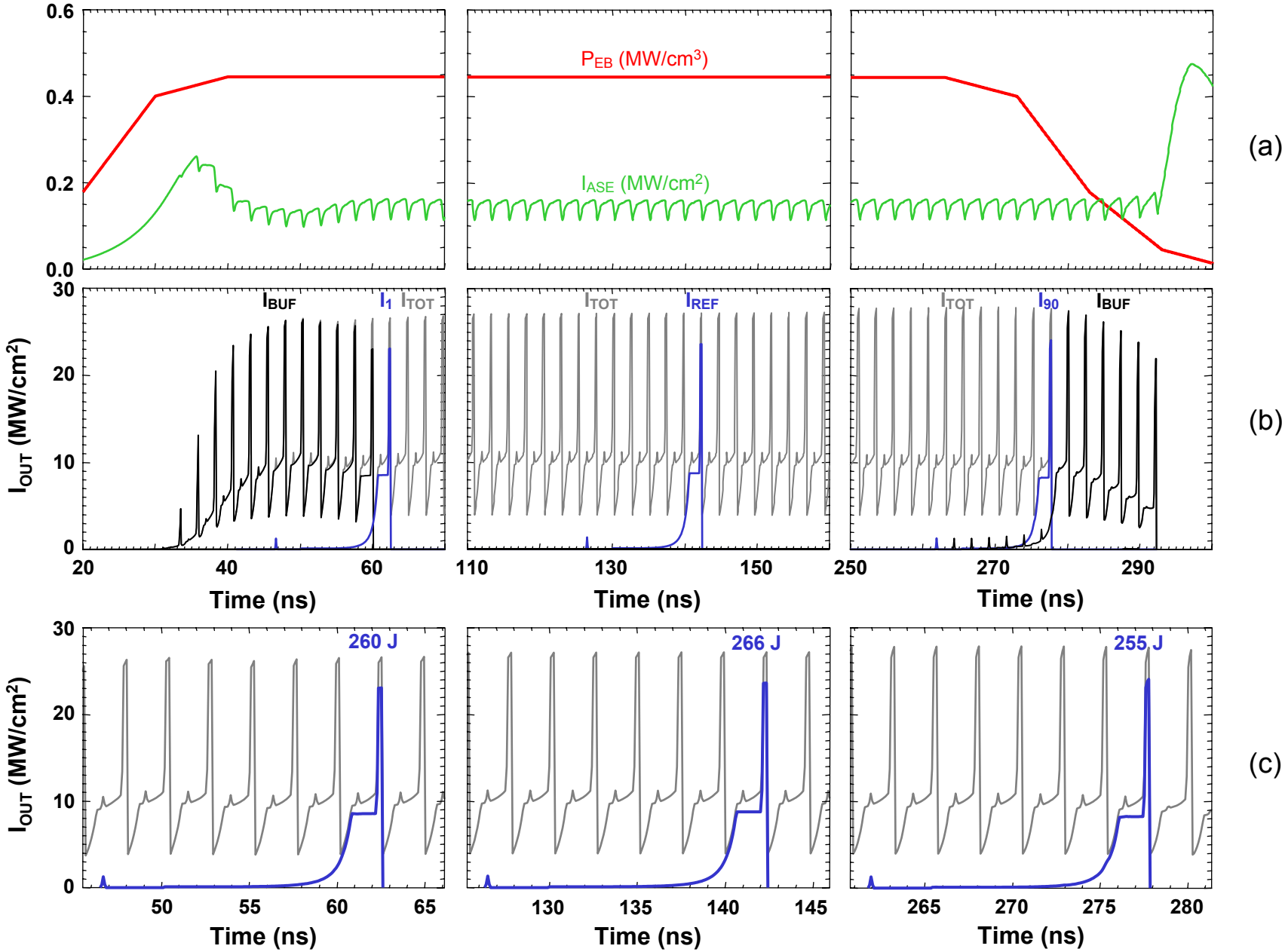

Fig. 6: (a,b) Simulated parameters at the final amplifier, showing selected output beams I_1, I_{REF}, I_{90} (blue), buffer beam I_{BUF} (black), total output intensity of all beams I_{TOT} (light grey), total ASE output I_{ASE} (green), and e-beam specific power deposition P_{EB} (red); (c) I_1, I_{REF}, I_{90} and I_{TOT} with magnified time scales.

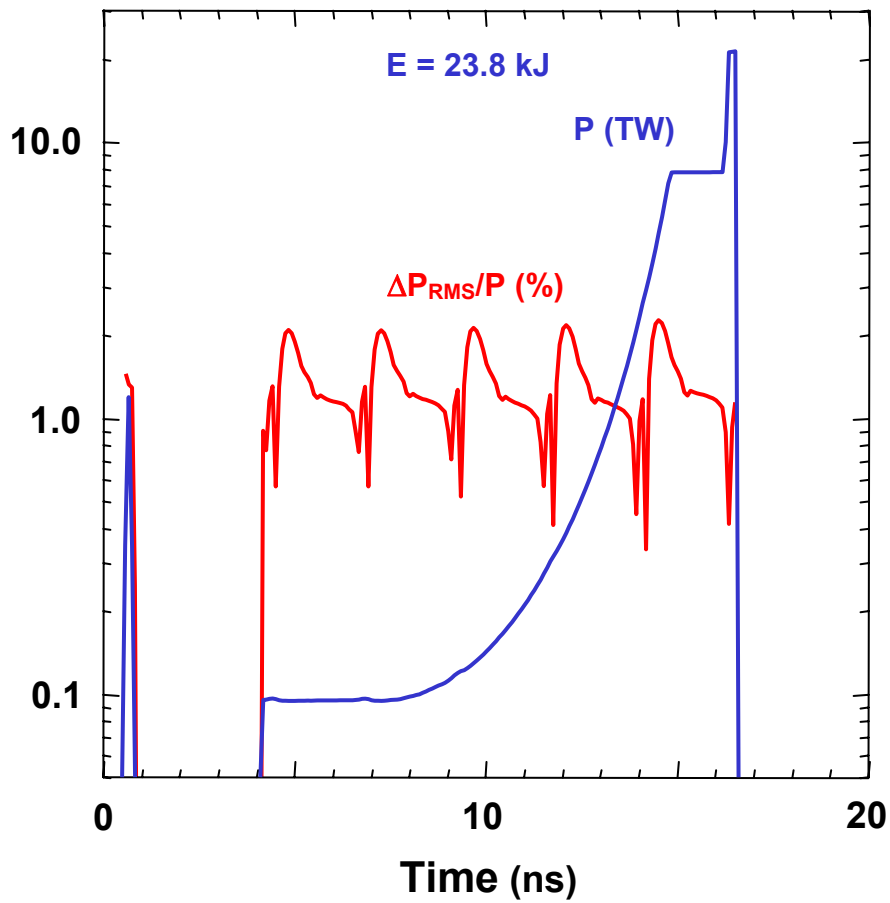

Fig. 7: Total instantaneous power in all 90 beams (blue) and fractional beam-to-beam RMS deviation (red) of the shock ignition pulse.

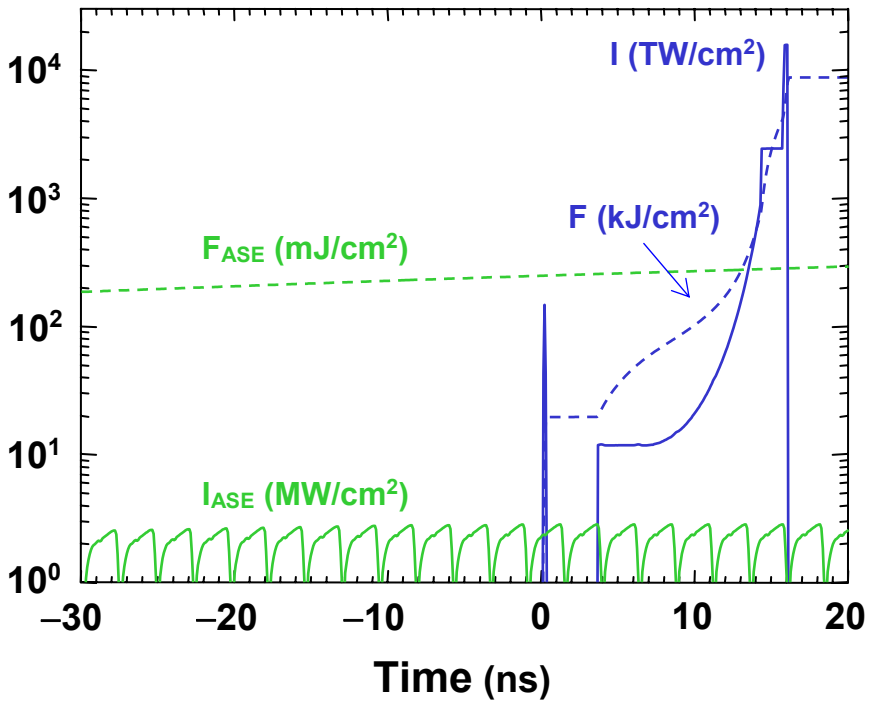

Fig. 8: Total on-target intensity (solid lines) and fluence (dashed lines) of the shock ignition pulse (blue) and ASE (green) from all 20 laser systems. The origin of the time scale is placed at the beginning of the picket pulse.

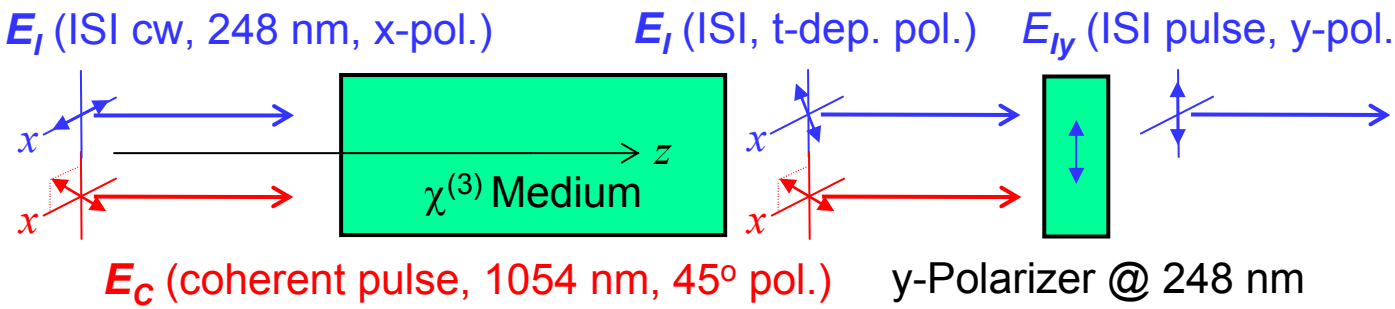

Fig. 9: Configuration of the proposed Kerr gate that uses an intense coherent 1 μm pulse to impose the desired pre-distorted envelope shape on a cw 248 nm ISI beam via polarization rotation.